Soft Matter

Accepted Manuscript

ROYAL SOCIETY OF CHEMISTRY

www.rsc.org/softmatter

Thermodynamics of Cell-Penetrating HIV1 TAT Peptide Insertion into PC/PS/CHOL Model Bilayers through Transmembrane Pore: the Roles of Cholesterol and Anionic Lipid †

Yuan Hu[a] **and Sandeep Patel**[*b]

Received Xth XXXXXXXXXX 20XX, Accepted Xth XXXXXXXXX 20XX
First published on the web Xth XXXXXXXXXX 200X
DOI: 10.1039/b000000x

Efficient delivery of pharmaceutically active molecules across cellular membranes using cell penetrating peptides (CPPs), such as the cationic human immunodeficiency virus-1 trans-acting activator of transcription peptide (HIV-1 TAT), continues to attract scientific attention in drug design and disease treatment. Experimental results show that the TAT peptide is not only capable of directly penetrating the biological membrane in a passive manner, but also forming physical, membrane-spanning pores that may facilitate transport. Experiments further show that anionic lipids accelerate peptide permeation within a range of mole percentage composition. In this work, we explored the structures and translocation thermodynamics of the cationic TAT peptide across a series of DPPC/DPPS model membranes with the presence of 0-30 mol % cholesterol. We computed the potentials of mean force by using umbrella sampling molecular dynamics simulations coupled to Martini coarse-grained force field. We systematically investigated the roles of cholesterol and anionic lipid (membrane surface charge) in TAT peptide translocation. In qualitative agreement with experimental findings, the barrier heights were significantly reduced in the presence of anionic lipids. A toroidal hydrophilic pore was strongly suggested by membrane structure analysis. Cholesterol stabilizes the liquid-ordered (Lo) phase of membranes and increases the elastic stiffness of bilayer. Consequently, it hinders transmembrane pore formation and thus modulates solute permeability, since the liquid-ordered phase suppresses reorientation of the lipid molecules on simulation time scales. Though cholesterol contributes marginally to the total free energy associated with peptide permeation, the coordination of cholesterol to the peptide weakens more favorable peptide-lipid interactions. Addition of the anionic lipid DPPS to the neutral DPPC bilayer leads to emergence and further enhancement of an interfacially stable state of the peptide due to the favorable peptide-anionic lipid interactions. Translocation free energy barriers decrease in lockstep with increasing DPPS composition in the model bilayers simulated. Finally, we investigated the size of hydrophilic pores emerging in our simulations, as well as qualitative mobility of the peptide on the membrane surface.

. See DOI: 10.1039/b000000x/

1 Introduction

HIV-1 TAT, the first protein transduction domain (PTD)[1,2] discovered in 1988, also known as a cell-penetrating peptide (CPP), has been constantly garnering significant attention in drug-delivery for nearly three decades. Experiments have shown that CPPs including the TAT peptide can traverse cell membranes alone or with molecular cargos of poor cellular permeability, such as semiconductor quantum dots (QDs)[3,4], DNA[5], RNA[6], vaccines[7], protein/peptide based pharmaceutics[8], nanoparticles[9], and even liposomes[10]. A wide arsenal of state-of-the-art techniques have been used to attack questions surrounding the binding and

† Electronic Supplementary Information (ESI) available: [The charge density and mass density profiles of the membrane systems, bond order parameter of the membrane in equilibrated condition, PMF contributions from water and cholesterols are included in the supplementary information.]

[a] *Merck Research Laboratories, 2015 Galloping Hill Road, Kenilworth, New Jersey 07033, USA.* [b] *Department of Chemistry and Biochemistry, University of Delaware, Newark, Delaware 19716, USA. Fax: 302-831-6335; Tel: 302-831-6024; E-mail: sapatel@udel.edu*

cellular internalization mechanisms, including labeled and label-free methods such as isothermal titration calorimetry (ITC)[11], single-molecule fluorescence microscopy[12], solid-state NMR (SSNMR)[13], time-of-flight mass spectrometry(MALDI-TOF MS)[14,15], lamellar neutron diffraction[16], second harmonic generation (SHG)[17], and so on. However, to the best of our knowledge, there is still a lack of understanding about the origins, selectivity, and structural and thermodynamic determinants of the cell-penetrating ability of these peptides.

Recent experimental studies[12,16,18] of live cells, cellular constructs, model membrane/lipid bilayers, and the like, frequently suggest pore-like membrane configurations as possible means for CPPs translocating across bilayer along with effects of ions and water flux. Kubitscheck *et al.*[12] systematically examined the permeation of a fluorophore labeled TAT peptide across the model giant unilamellar vesicles (GUVs) by using high-speed single-particle tracking (SPT) and confocal laser scanning microscopy (CLSM). The authors discovered no TAT peptide translocation in pure phosphatidylcholine (PC) and cholesterol (CHOL) only GUVs, even at high concentrations. However, they showed that systematically increasing the phosphatidylserine (PS) content in PC lipid bilayers dramatically increased the permeability of the TAT peptide. The TAT peptide was able to rapidly translocate into PC, PS and cholesterol mixed GUV with a critical threshold of 40 mol % anionic PS component. Peptides directly translocated into GUVs in a passive manner. The efflux experiments of tracer molecules suggested that TAT peptide translocation may be associated with formation of an intramembrane pore estimated to be 1.3 nm $\sim$ 2.0 nm.

Acknowledging the work of Kubitscheck et al[12] on the clean vesicle systems, we used molecular dynamics simulations (MD) to understand the selectivity of TAT translocation across PC/PS/CHOL systems from the perspective of structural and thermodynamic features at the microscopic level. We constructed several model lipid systems to interrogate the role of cholesterol and anionic lipid components in a systematic manner. First we compared the dependence of cholesterol in pure PC or PS systems with 0-30 mol % cholesterol. Then, we investigated the correlation of anionic PS lipids with the TAT peptide translocation into DPPC/DPPS mixed lipid bilayers with 0 or 20 mol % cholesterol, which were used to reproduce the membrane compositions studied by Kubitscheck et al[12]. Specifically, we used the umbrella sampling (US) method utilizing the most widely applied MARTINI coarse-grained (CG) force field to estimate the free energetics for transferring the cationic TAT peptides from bulk aqueous-like environment to the hydrophobic center of the bilayer. We discuss the results in two parts: 1) the effect of cholesterol composition, 2) the role of anionic lipid component in TAT translocation into model lipid bilayers. The results of the potentials of mean force (PMFs), effect of different conformations, and PMF contributions from the system components have also been discussed in each section. We aim to recapitulate the experimental observation with CG models. At the very least, we seek to explore the qualitative trend in free energetics and further obtain molecular level insight into CPP translocation.

2 Methods

The Martini Coarse-grained (CG) model has been successfully used to study soft matter and membrane biophysics, such as lipid/surfactant self-assembly, vesicle formation and fusion, peptide-membrane binding, nano-particles and short peptides translocation, and so on[19–22]. The force field maps four consecutive heavy atoms of a molecule at an atomic resolution to one bead, except for ring-like structures. It considers four main types of interaction sites such as polar (P), nonpolar (N), apolar (C), and charged (Q). Moreover, within a main type, subtypes are used to distinguish the hydrogen-bonding capabilities (d = donor, a = acceptor, da = both, 0 = none) or the degree of polarity (from 1 = low polarity to 5 = high polarity). Since the diffusive motion for water in CG model is the same as in all-atom (AA) models but that four water molecules are mapped to one CG water, the effective simulation time in the CG model is generally rationalized to be approximately four times as large as that in AA model[23]. Although the resolution is reduced in Martini model due to neglecting atomic details, the CG force field is still sufficient to reproduce and predict structural and free energetic behaviors[24,25]. The Martini force field with Particle Mesh Ewald (PME) is shown to provide a more realistic description of the interaction of charged molecules with lipid membranes and is also found necessary to induce and accommodate transmembrane pores during solute translocation, although the use of PME is not the standard method[26,27].

In this work, we used the latest non-polarizable Martini coarse-grained (CG) model developed by Marrink et al[23,28,29] to simulate interactions among system components, such as peptides, lipids, cholesterols, water and ions. We used the TAT protein transduction domain (PTD) fragment corresponding to amino acids 48 to 57 of the domain of HIV-1 TAT protein (Gly-Arg-Lys-Lys-Arg-Arg-Gln-Arg-Arg-Arg, +8 charges). The N-terminus and the C-terminus of the TAT peptide were considered as neutral, and all the backbones were represented by P5

beads as widely used in this CG model[19,20,30–32]. 1,2-dipalmitoyl-sn-glycero-3-phosphocholine (DPPC), 1,2-dipalmitoyl-sn-glycero-3-phospho-L-serine (DPPS) lipids and cholesterols were used as the building blocks of the model bilayers. In Martini, the DPPC lipid is made of four head group beads and eight tail beads. The DPPS lipid structure and parameters are the same as the DPPC lipid except that the head group choline changes from positively charged (type Q0) to neutral bead (type P5) to represent serine[21]. Fig. 1 illustrates the CG structures of HIV-1 TAT peptide, water, ions, cholesterol, DPPC and DPPS lipids used in the framework of the Martini force field and the simulation system cells.

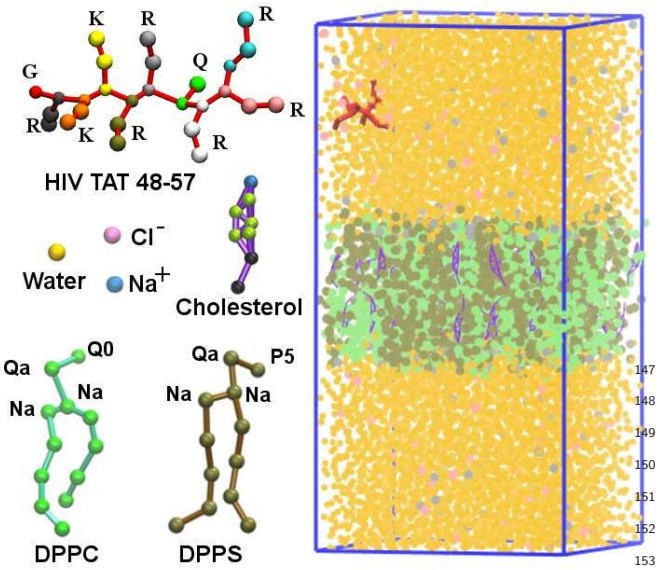

Fig. 1 Structures of Coarse-Grained (CG) cholesterol, DPPC, DPPS, and mixed bilayer, water, ions, and TAT, and a typical lipid mixture system.

2.1 Simulation Protocol

All the MD simulations were carried out using MPI supported GROMACS software package (version 4.6.3), single precision. The simulation cell consists of a rectangular box. We constructed 14 systems including DPPC or DPPS only systems with 0-30 mol % cholesterol, and 0-100 mol % DPPS systems with 0-20 mol % cholesterol. The system compositions are summarized in Table 1. Each cholesterol-free system, such as the DPPC only system, contains 1 TAT peptide, 256 lipid molecules (128 lipids per leaflet), surrounded by 7554 water and 150mM NaCl ions (82 sodium and 82 chloride ions). The systems containing cholesterol and/or DPPC/DPPS mixture were constructed by substituting DPPC to DPPS and cholesterol equally from both leaflets. Water molecules were replaced to counter-ions when necessary to keep the system charge neutral.

Table 1 Composition of systems modelled. Each system includes one TAT peptide (+8 charges), which is not shown in the table.

Ratio[a]	CHOL	DPPC	DPPS	Water	Na^+	Cl^-
0: 100: 0	0	256	0	7554	82	90
10: 90: 0	26	230	0	7544	82	90
20: 80: 0	52	204	0	7554	82	90
30: 70: 0	76	180	0	7554	82	90
0: 75: 25	0	64	192	7362	274	90
0: 50: 50	0	128	128	7426	210	90
0: 25: 75	0	192	64	7490	146	90
20: 60: 20	52	152	52	7502	134	90
20: 40: 40	52	102	102	7452	184	90
20: 20: 60	52	52	152	7402	234	90
30: 0: 70	76	0	180	7374	262	90
20: 0: 80	52	0	204	7350	286	90
10: 0: 90	26	0	230	7314	312	90
0: 0: 100	0	0	256	7298	338	90

a: Ratio of CHOL:DPPC:DPPS

We first minimized each lipid system with the steepest descent method and then equilibrated it under constant particle, pressure and temperature (NPT) ensemble molecular dynamics simulations for 1μs at 1 atm. Since the phase transition temperatures of DPPC and DPPS are 314 K and 326 K, respectively, we carried out all the simulations at 350 K. This temperature setting is also carefully tested and suggested by the all atom simulations Cascales' et al[33]. We used a time step of 20 fs and updated the neighbor list every 10 steps. The Lennard-Jones (LJ) and electrostatic (Coulomb) interactions were calculated by using simple spherical cutoff at a distance of 1.2 nm with a smooth switching function of distances 0.9 nm and 0.0 nm, respectively. The conditionally convergent long range electrostatic interactions were modeled by using the PME method with a fourth-order spline and a 0.12 nm grid spacing. The relative dielectric constants were set to 15 for use in combination with the non-polarizable water force fields. To maintain the temperature at 350 K, we used the velocity rescaling scheme with time constants of 1.0 ps. We used two temperature coupling groups: water and ions were considered as one, and the remaining atoms were set as the second group. We used the Parrinello-Rahman coupling scheme with 12.0 ps to maintain the pressure of 1 atm for the systems. To keep the bilayer in a tensionless state, periodic boundary conditions with a semi-isotropic pressure

coupling algorithm with a 3.0×10^{-4} bar^{-1} compressibility was used. The LINCS algorithm[34] was used to apply the bond constraint present in Martini force fields.

2.2 Umbrella Sampling Simulations

To obtain a PMF for the transfer of TAT in each system, we used 61 umbrella sampling (US) windows ranging from 0.0 to 6.0 nm at a spacing of 0.1 nm along our chosen reaction coordinate (Rxn. Coord.) ξ, which is the z-dimension distance between the center of mass (c.o.m.) of peptide and c.o.m of the membrane (here the whole membrane including DPPC, DPPS, and CHOL). We first generated initial configurations in the windows along the specified Rxn. Coord. by growing a TAT peptide in the center of the above equilibrated systems, and further equilibrated the peptide-bilayer-water-ion system for about 200 ns. In order to prevent the unnecessary drift of the membrane in the direction of the membrane normal, we applied a position restraint, along the z-dimension, with a force constant of 1000 kJ/mol/nm^2 on the charged groups (NC3, PO4) of lipid molecules during the peptide growing-in phase in all simulations. In this work, the membrane interface is defined as the intersection region of the headgroup and solution mass density profiles (the mass density profiles are shown in Fig. S2 in SI). The interface is estimated at 2.0 nm from the center of the bilayer in all systems. The membrane thickness is approximately 4.0 nm. For US MD simulations, we applied harmonic potentials with a force constant of 1500 kJ/mol/nm^2 to restrain the peptide at each window. Each window was simulated for 600 ns, and the total simulation time period was 36.6 μs. The details of the window setup and US method have been described in our recent work[19].

The weighted histogram analysis method (WHAM) was used for post-simulation unbiasing of umbrella sampling data[35]. We used the Gromacs tool 'g_wham' to generate the final PMF. The Visual Molecular Dynamics (VMD) package[36] was used to monitor the simulation, visualization and graphics preparation for this work.

2.3 System Component Contributions in Potentials of Mean Force

The contribution to the total PMF from the system component, α, (i,e α = water molecules, α = lipids, α = ions, α = cholesterols) is:

$$W_\alpha(\eta) \;=\; -\int_{\eta_0}^{\eta_1} d\eta \;\left\langle F^{\alpha}_{z,peptide-com}\right\rangle_{\eta} \qquad (1)$$

where η_0, η_1 is the value of the Rxn. Coord. in the reference state, η is the dummy variable of integration, $\left\langle F^{\alpha}_{z,peptide-com}\right\rangle_{\eta}$ is the average z-component of the total force on the peptide center of mass arising from interactions with system component α. The total PMF is a sum over the system component contributions:

$$W(\eta) \;=\; \sum_{\alpha} W_\alpha(\eta) \qquad (2)$$

The instantaneous force on the peptide from system component α, $F^{\alpha}_{z,peptide-com}$, was computed post-simulation by processing the trajectories of each US window using the Gromacs 'mdrun_mpi' module. We excluded the interactions between the peptide and system components other than α. The details of the PMF decomposition have been described in the Appendix of our recent work[24].

The final PMF and its standard error (uncertainty) were estimated by block averaging consecutive 100 ns time periods from the production run of each US window[37](The first 100 ns data are not used). We ensured that the block size was significantly larger than the correlation time in each umbrella window.

3 Results and Discussion

3.1 Cholesterol Dependence: 0-30 mol % CHOL in PC or PS systems

Cholesterol is a small molecule composed of four rings with one hydroxyl group and one hydrocarbon chain, where the hydroxyl group is hydrophilic and the rest is hydrophobic. Cholesterol is an essential component of mammalian cell membranes, generally, present around 20 mol % in cells[38]. Cholesterol facilitates cell signaling processes and assists in local lipid domain (raft) formation[39]. It plays a major role in maintaining membrane structural integrity and fluidity of cell membranes[40–46]. The amphipathicity of cholesterol confers on it structural facility to align with phospholipids, and the planar and effective rigidity accommodate its ability to complementarily pack within the membrane, thus increasing bilayer order[47]. Paradoxically, cholesterol increases the fluidity of membranes, as a result of its rapid flip-flop between the leaflets inside the bilayers[48,49].

3.1.1 Potentials of Mean Force (PMFs) of TAT Translocation in Systems of Varying Cholesterol (CHOL) Concentration Fig. 2 shows the PMFs of TAT translocation into PC or PS systems with different mole concentrations of cholesterol along the Rxn. Coord. ξ, which is the z distance between the center of mass

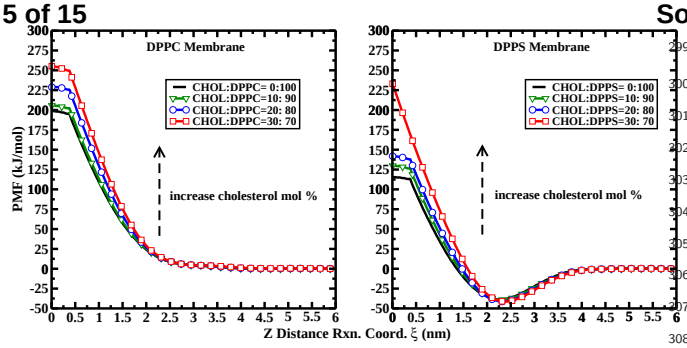

Fig. 2 PMF's of TAT translocation into model DPPC (left) and DPPS (right) lipid bilayers with different cholesterol (CHOL) percentage.

(c.o.m.) of the peptide and c.o.m. of the entire membrane. The peptide passes from bulk water (ξ=6.0 nm) to bilayer center (ξ=0.0 nm). The left panel shows the translocation free energies in zwitterionic DPPC membrane, and the right panel in anionic DPPS systems. In both zwitterionic and anionic lipid bilayers, the TAT peptide moves freely in the bulk water, where there is no free energetic difference as the Rxn. Coord. ξ ranges from 4.0 nm to 6.0 nm. However, at the membrane interface, the TAT peptide behaves differently in these two types of lipid systems. It does not strongly bind to the zwitterionic/neutral lipid bilayer interfaces, where no free energy minima are observed. In contrast, the TAT peptide strongly binds to the anionic lipids as indicated by a PMF minimum of -40 kJ/mol. This is in qualitative agreement with results of experiments[13,16,17,50] and simulations[51,52]. Similar lipid association preferences are observed for other CPPs such as nona-arginines[19,20,53,54]. This favorable peptide binding in anionic lipid systems is mainly because of the strong electrostatic interactions between cationic TAT peptide with eight positive charges and the high density of negative charges of the membrane at the interface (see the charge density profiles of the DPPC and DPPS membrane systems in SI Fig. S1). We further notice that the molar concentration of cholesterol doesn't affect the depth of the free energy minimum at the interface of both zwitterionic and anionic lipid bilayers (see the results in Table 2), which implies that the enrichment of cholesterol in the membrane doesn't affect CPP association at a moderate cholesterol mole fraction. This can be understood by the fact that cholesterol molecules are mainly located inside the membrane near the hydrophobic core, and they almost have no effect on surface charge density (see the density profiles in SI Fig. S2), the latter because cholesterol is neutral, and because the electrostatic components of peptide-membrane interaction dominate over other dispersion and non-bonded interaction forces.

Although, interface properties are not affected by the amount of cholesterol in the systems, the overall translocation free energy barrier increases as higher mole concentration of cholesterol is incorporated into membranes.Addition of cholesterol increases order of lipid tails (see the bond order parameter of DPPC, DPPS in SI Fig. S3), inducing more rigidity into our model membranes much like experimentally observed induction of the liquid-ordered (Lo) phase of membranes and increases elastic stiffness; increased stiffness works against peptide translocation by reducing membrane/bilayer deformability to form 'pore-like' configurations conducive for the peptide states in the center of the bilayer. Higher cholesterol fraction in the membrane impedes peptide translocation. Experiments show that cholesterol depletion facilitates peptide translocation[55]. We note that the change in the curvature of the PMF's with increasing cholesterol content may be connected to an increasing elastic deformation penalty contribution described by a Helfrich-type model of membrane fluctuations. To first order, assuming equivalent global curvatures (extrinsic and Gaussian), differences in the steepness of the PMF curves may be related to some stiffness or rigidity property of the membranes we model. Connecting the angstrom-scale deformations we see in our simulations with curvature changes via Helfrich-type analysis may provide further insight into quantitative changes in membrane bending rigidities. This work continues as a further avenue of inquiry.

Furthermore, for the PC and PS systems with the same mole concentration of cholesterol, lower free energy barriers are observed in the PS systems. The free energy barrier is about 200-250 kJ/mol in PC membrane systems, and 115-235 kJ/mol in the PS membrane systems, respectively. There is 20 to 100 kJ/mol less free energy cost in the PS systems due to the favorable lipid-peptide interactions. Noteworthy is that most of the PMFs (except DPPS with 30% cholesterol) have a kink at around 0.5 nm of the Rxn. Coord. ξ. The PMFs flatten as the peptide moves toward the center of the bilayer from this kink position. As discussed in our recent work[19], the flattened region corresponds to the formation of a transmembrane pore-like structure induced by the cationic peptide. Fig. 3 shows snapshots of the pore and defect structures in DPPC and DPPS systems with different cholesterol mole concentrations. The lack of a kink in the PMF of the DPPS membrane system mixed with 30 mol% cholesterol in Fig. 2 is due to the fact that no stable water pore was formed. This is shown clearly in Fig. 3. Once the pore is formed in the DPPS systems, the peptide can move through the pore with insignificant free energy

Table 2 Analysis of PMF's for TAT translocation across the PC or PS membranes with different mole fraction of cholesterol (PMF's in units of kJ/mol). The table includes the free energy barrier of peptide translocation from bulk to center (ΔG_{total}), the interfacial free energy minima relative to the bulk (ΔG_{min}) and the maximum free energy barrier from the free energy minimum to the center of the bilayer (ΔG_{max}).

Ratio[a]	ΔG_{total}	ΔG_{min}	ΔG_{max}	Error
0: 100: 0	198.5	-	198.5	1.0
10: 90: 0	205.6	-	205.6	1.1
20: 80: 0	228.9	-	228.9	0.5
30: 70: 0	255.1	-	255.1	1.2
0: 0: 100	115.3	-38.6	153.9	0.7
10: 0: 90	129.8	-39.1	168.9	1.0
20: 0: 80	141.8	-41.2	183.0	1.6
30: 0: 70	233.2	-41.4	274.6	1.3

a: Ratio of CHOL:DPPC:DPPS

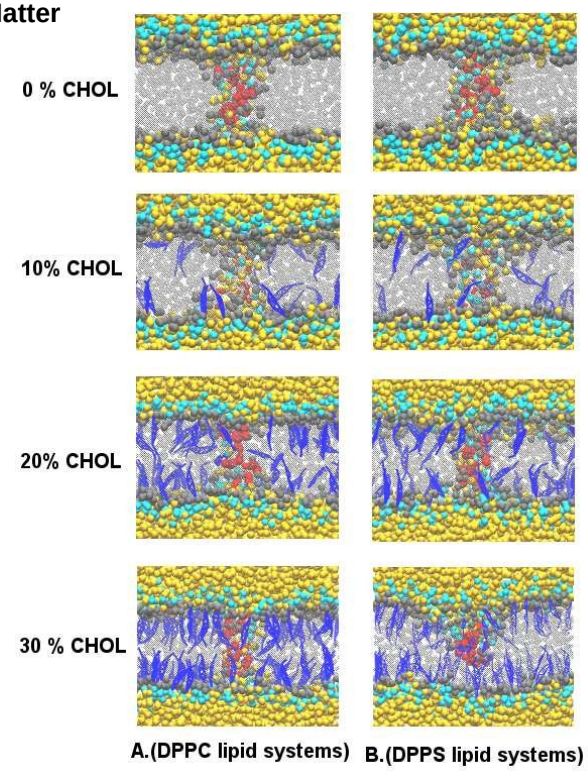

Fig. 3 Snapshots of the center windows in 0-30 mol % cholesterol systems. Red, yellow, cyan and gray spheres represent the TAT peptide, water, phosphates and carbonyls, respectively. Cholesterol is shown in blue.

penalty. Table 2 summarizes the free energy barriers of different systems. The intrinsic pore formation free energy is highly correlated with membrane thickness as discussed in other work[54,56].

3.1.2 PMF Decomposition: Systems with Varying Cholesterol Composition To scrutinize the roles of cholesterol and other system components, we decompose the PMFs into the contributions of the components in the peptide-membrane systems, shown in Fig. 4. The sum of the component contributions matches the calculated PMF obtained from WHAM analysis (see Fig. S4 in SI). In both PC and PS systems, cholesterol contribution increases with increasing cholesterol mole percentage. However, the increments of the barrier in DPPS systems are slightly smaller than those in DPPC systems. Specifically, cholesterol components contribute to the barrier about 3 to 30 kJ/mol free energy in the DPPC systems, but only up to 25 kJ/mol in DPPS systems. Generally, increasing the concentration of cholesterol in the membrane disfavors peptide translocation. Nevertheless, compared to the total peptide translocation barrier, the contribution from cholesterol is very small, and the differences between PC and PS systems are negligible. Although cholesterol's contribution to the total PMFs is relatively small, it significantly affects stabilization of the TAT peptide inside the membrane. The small molecular size and relatively rapid diffusion of cholesterol in the interior of the bilayer allow it to easily associate with the peptide. Fig. 5 shows the amount of cholesterol around the TAT peptides in the first solvation shell (the width of the solvation shell was defined as 0.67 nm from all the beads of the peptide, and it has been chosen by the calculation of pair correlation functions between the peptide and water beads[19]). As more cholesterols associate with the TAT peptides, and the number of negatively charged phosphates around the cationic peptide consequently decreases (see Fig. 6), peptide-lipid interactions are eventually weakened.

Fig. 7 shows the contribution to the PMFs from the lipids and all ions (including counter-ions of peptides and lipids) in the PC and PS lipid systems. These non-aqueous components confer thermodynamic stability for the peptide in the bilayer center in both PC and PS systems. However, this effect is reduced significantly as cholesterol molecules are added to the systems. With cholesterol at 30 mol %, overall stablization is damped to zero in the DPPS systems, and becomes destabilizing in the DPPC systems.

In both PC and PS systems, the cholesterol and lipid-ion contribution stabilizes the peptide in the interface region. Minima are found in all cholesterol contributions. Cholesterols stabilize the peptide at the interface, and favor peptide association. However, this association reduces the stabilization from lipids, and results in roughly

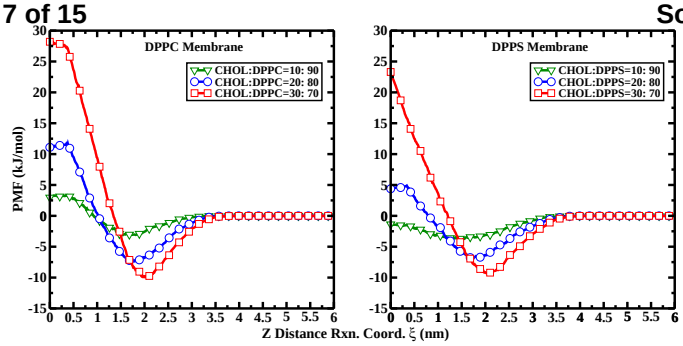

Fig. 4 PMF decomposition showing cholesterol contributions to total PMF for TAT translocation into model DPPC (left) and DPPS (right) lipid bilayers with different CHOL percentages.

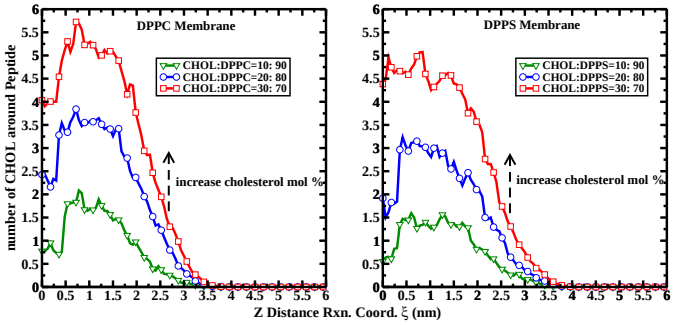

Fig. 5 Number of cholesterol molecules in shell surrounding TAT peptide

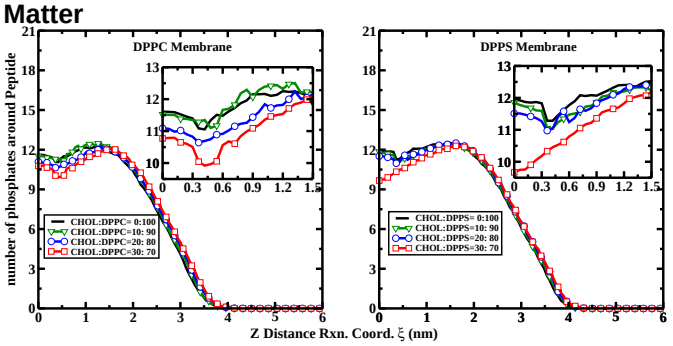

Fig. 6 Number of phosphates groups surrounding TAT peptide

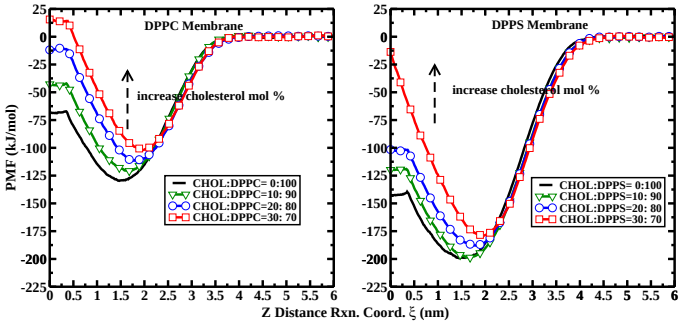

Fig. 7 PMF decomposition showing sum of lipid (DPPC or DPPS) and ion (Na^+ and Cl^-) contributions to TAT translocation into model DPPC (left) and DPPS (right) lipid bilayers with different CHOL percentages.

no change of the peptide association in the membrane interface. At bilayer center, cholesterol increases the barrier of TAT translocation at high mole fractions, and contributes an overall destabilization effect. The weakened stabilization effect of lipids is attributable to replacement of stabilizing lipid groups in the peptide solvation shell.

3.2 Anionic Lipid Component Dependence: PC/PS systems with 0-20 mol % cholesterols

Certain experiments[55,57] and simulations[58–60] suggest that higher membrane cholesterol content reduces accumulation of the peptides in the membrane, and that CPPs prefer to penetrate via regions containing less cholesterol, these regions being supposedly of lower rigidity and more facile to deform possibly in order to accommodate peptide translocation. The above simulations of cholesterol-dependence in neutral and anionic lipids recapitulate this observation; they further indicate that the cholesterol contribution solely relies on the mole concentration in the membrane composition, which is independent of the lipid charge states. Note that translocation barriers of the TAT peptide are relatively lower in the anionic lipid systems. Experimental results show that in 20 mol % cholesterol and PC/PS mixed giant unilamellar vesicles (GUVs), rapid translocation of the TAT peptides was detected at 40 mol % DPPS composition. These experiments further suggest nanometer-size pores are involved via tracing fluorescent molecule leakage[12]. To investigate the role of membrane surface charge in peptide internalization, we constructed a series of PC/PS mixed lipid bilayer systems with 20 mol % cholesterol varying the mole percentage of PS lipids from 0 mol % to the maximum 80 mol %. The corresponding cholesterol-free systems with the same ratio of PC:PS were also constructed.

We computed PMFs of the TAT peptides from the the bulk water (ξ=6.0 nm) to the center of the bilayers (ξ=0.0 nm). Fig. 8 shows the PMFs of TAT translocation into CHOL/PC/PS membranes (left panel), and PC/PS mixed membranes (right panel) along the Rxn. Coord. ξ (the z distance between the c.o.m. of the peptide and the c.o.m of the membrane). The results are summarized in Table 3. The barrier from bulk to the center of the bilayer is significantly reduced by a factor

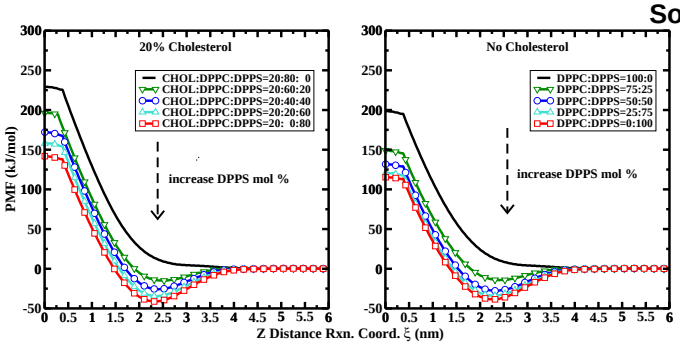

Fig. 8 PMFs of TAT translocation into model DPPC/DPPS mixed lipid bilayers with 20 mol % cholesterol (left panel), and 0 mol % cholesterol (right panel). The same PC:PS ratio is used in both systems, which is 4:0, 3:1, 2:2, 1:3, 0:4. The dashed arrow indicates the direction of increasing PS mole concentration.

of two with increasing mole percent of PS in the membrane. Specifically, by varying the ratio of PC:PS from 4:0 to 3:1, 2:2, 1:3 and 0:4, in the 20 mol % cholesterol systems, the free energy cost changes from around 230 kJ/mol to only 142 kJ/mol; in the cholesterol-free systems, the translocation barrier decreases even more to 115 kJ/mol. This trend agrees qualitatively with experimental observations[55,57,61,62]. Unsurprisingly, in the cholesterol-depleted membrane systems, the free energy barrier is much lower.

Fig. 8 shows that the addition of PS into the PC bilayer gives rise to an interfacial free energy minimum and the depth of the minimum is further enhanced with increasing PS concentration. It indicates that although there is no strong association between the TAT peptide and neutral lipid bilayers, increasing the surface charges, such as adding anionic lipids into the membrane composition, can significantly enhance the peptide interfacial binding. Comparing the depth of the minima of the systems with the same PC:PS ratio in Table 3, we noticed that the 20 mol % and 0 mol % cholesterol mixture systems show almost quantitatively the same surface association and binding preference. It again implies that the interface properties are not affected by the amount of cholesterol in the systems, but rather the surface charges. Relating to a possible mechanistic rationale for the CPP translocation, strong peptide association will increase the local concentration of the peptide at the membrane surface. As a result, it may increase the number of translocation events with a relatively larger interfacial sample population, and further increase the translocation probability which manifests in observable internalization rates.

Table 3 The free energetic results of TAT PTD translocation across the PC/PS mixed membrane with 20 mol % cholesterol and no cholesterol (in units of kJ/mol). The table includes the free energy barrier of peptide translocation from bulk to center (ΔG_{total}), the interfacial free energy minima relative to the bulk (ΔG_{min}) and the maximum free energy barrier from the free energy minimum to the center of the bilayer (ΔG_{max}).

Ratio[a]	ΔG_{total}	ΔG_{min}	ΔG_{max}	Error
20: 80: 0	228.9	-	228.9	0.5
20: 60: 20	196.1	-15.0	211.1	1.5
20: 40: 40	172.1	-25.8	197.9	1.3
20: 20: 60	157.9	-34.5	192.4	1.4
20: 0: 80	141.8	-41.2	183.0	1.6
0: 100: 0	198.5	-	198.5	1.0
0: 75: 25	148.9	-14.3	163.2	1.6
0: 50: 50	131.7	-27.8	159.5	0.8
0: 25: 75	120.7	-34.0	154.7	0.9
0: 0: 100	115.3	-38.6	153.9	0.7

a: Ratio of CHOL:DPPC:DPPS

3.2.1 Pore Formation and Water and Ion Flux

Our simulation results so far indicate (see Fig. 2 and Fig. 8) that despite large free energy barriers, there are structural factors that contribute in a stabilizing manner as a CPP translocates into the membrane center. This is particularly suggested by Fig. 2 showing the flattened regions of TAT translocation into bilayers of varying cholesterol concentration. This flattening of the PMF, as we[19,20,54] and others[37,63–67] have discussed in previous work, is intimately related to structural deformations of the bilayer-water configurations that accommodate transmembrane pore structures. From snapshots of the molecular dynamics simulations where the peptide is in the center of the bilayers (Fig. 9), we can see hydrophilic pores are induced in both 20 mol % cholesterol and cholesterol-depleted membrane systems. The membrane headgroups reorient to the rim of the channel, and the headgroup-peptide interactions stablize the peptide inside the membrane. Water and ions solvated the peptide inside the pore, freely flowing through the pore and exchanging with the bulk solution. The kink positions of the PMFs in Fig. 8 show the maximum distance between the c.o.m. of the peptide and the c.o.m. of the membrane where the pore is readily generated and stable throughout the lifetime of the extended MD simulations we generate. The variation of the mole percentage of anionic lipids doesn't affect the kink positions in both types of systems.

The average pore configurations are further investigated by computing the density profiles of the membrane

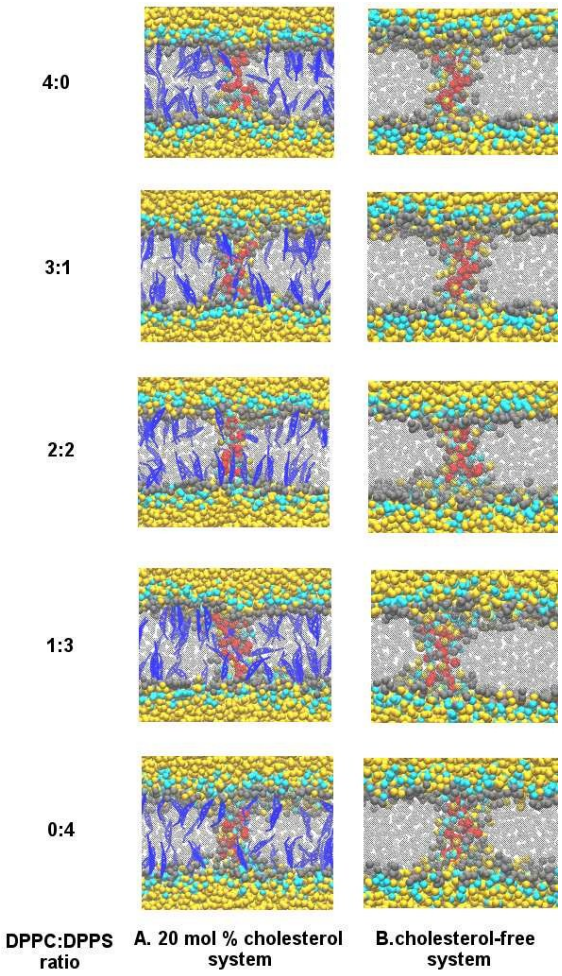

Fig. 9 Snapshots of the center windows in DPPC/DPPS mixed membrane systems with 20 mol % cholesterol or no cholesterol. The same color coding is used as for Fig. 3.

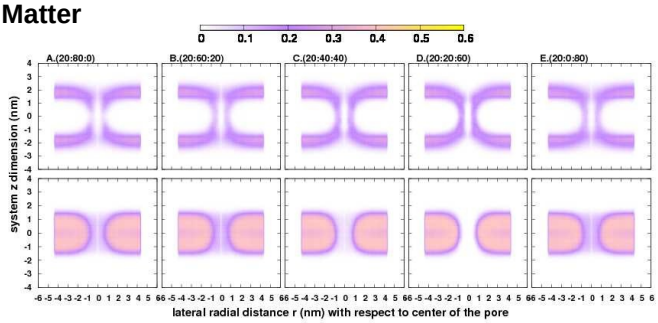

Fig. 10 Two-dimensional density profiles $\rho(r, z)$ of (top panels) lipid head groups, and (bottom panels) tails for the TAT peptide penetrating into the center of the bilayer. All the profiles are computed from the 20 mol % cholesterol systems (A-E columns), and ploted as a function of the lateral radial distance with respect to the center of mass of the peptide (r) and the system z dimension. The number in the bracket of each column shows the CHOL:DPPC:DPPS ratio of the membrane composition.

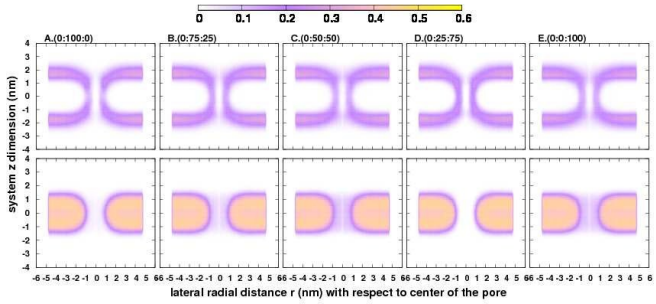

Fig. 11 Two-dimensional density profiles $\rho(r, z)$ of (top panels) lipid head groups, and (bottom panels) tails for the TAT peptide penetrating into the the cholesterol depleted systems (A-E columns). The number in the bracket of each column shows the CHOL:DPPC:DPPS ratio of the membrane composition.

along the lateral dimension. Fig. 10 and Fig. 11 show the densities of lipid head groups and tails. The pore shape and channel size differ slightly upon changing PS or cholesterol content. The lipids deform to a toroidal shaped pore, and the head groups reside on the rim of the pores. Furthermore, the narrow neck of the pore diameter is around 1.5 to 2.0 nm, which coincides with an experimental estimation of the pore size[12].

3.2.2 PMF Decomposition of TAT translocation in Different DPPS Concentration Systems Apart from pore formation, anionic lipids play an important role in the TAT peptide translocation. High mole percentage of PS in the membrane composition significantly reduces the free energetic barrier of the peptide internalization. Cholesterol depletion further enhances the trafficking of peptide across the membrane. Here, we again decompose the PMFs into the contributions of different components to investigate the associated free energetic dependencies. The sum of the component contributions is validated with the calculated PMF obtained from WHAM analysis (see Fig. S5 in SI).

Strong force-field based electrostatic interaction between ions and peptide help maintain the peptide solvation and stabilize the peptide in the aqueous water solution. However, when the peptide moves from the hydrophilic environment to the hydrophobic core of the membrane, the decrease in local salt concentration incurs large free energy penalty. The penalty is around 250 kJ/mol in the DPPC bilayers with 20 mol % or no cholesterol systems, as shown in Fig. 12 (see the black

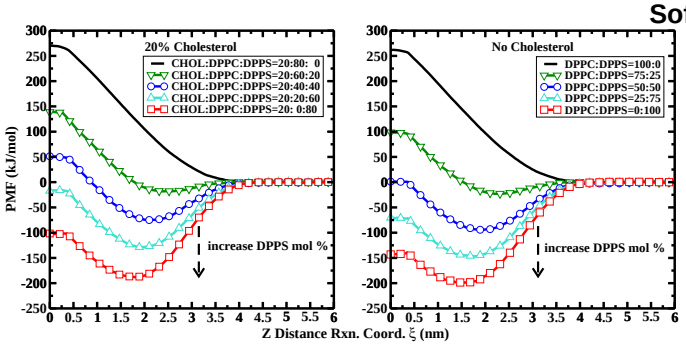

Fig. 12 Total PMF contribution from DPPS and ions (Na^+ and Cl^-) in 20% CHOL and no CHOL mixture systems.(note: water and DPPC contributions are not included in each curve.)

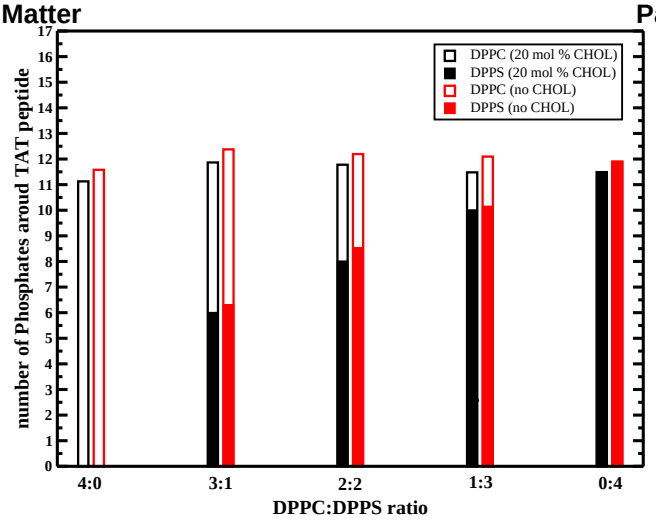

Fig. 13 Total number of phosphates in the first solvation shell of DPPC and DPPS in various PC:PS ratio systems. Black bars represent the 20 mol % cholesterol systems, and red bars represents cholesterol-free systems. The filled portions of the bars represent contribution from the phosphates from DPPC, and the unfilled are from the phosphates of DPPS.

solid curves with no symbols). This is also qualitively consistant with the salt effect in the internalization of nonaarginine, which is another CPP molecule we studied previously[19]. Similar to the ions, another large destabilization penalty comes from water desolvation (shown in SI Fig. S6). After mixing DPPC with the DPPS membranes, the contributions of the ions together with the DPPS start to decrease. The strong stabilization effect from DPPS compensates the desalting effect and gives roughly an overall 100 kJ/mol stabilization free energy in 20 mol % cholesterol systems, and around 150 kJ/mol in the cholesterol-free systems after replacing all the DPPC lipids with DPPS. This agrees with previous simulation results in that both DPPC and DPPS are stabilizing CPP translocation. The stabilization mainly comes from the strong charge interactions between DPPS and the TAT peptides carrying 8 positive charges. In Fig. 13, we can see the coordination number of the negatively charged phosphates from DPPS in the first solvation shell of the TAT peptide continuously increases along with the mole percentage growth of DPPS, whereas the number of phosphates from DPPC coordinating to the peptide is gradually reduced.

Fig. 14 shows the total contribution from the membrane and ions containing DPPC, DPPS, Na^+ and Cl^- ions. The favorable interactions from DPPS reduce the barriers and contribute an overall stabilization effect. This can be attributed to the large amount of net negative surface charges in the anionic PS lipid systems compared to neutral PC lipids. However, in the systems containing cholesterol, the slightly weaker stabilization effect is due to the cholesterol binding to the peptides and reducing the density of lipids around the peptides. The cholesterol itself contributes a relatively small amount (4-12 kJ/mol) of destabilization effect (see Fig. S7 in SI). Furthermore, adding cholesterol to the membrane increases the order of both DPPC and DPPS lipid molecules. Fig. 15 shows the average orientational bond order parameter P_2 of the lipid tail bonds, which is calculated from the average second-rank Legendre polynomial, $< \frac{1}{2}(3cos^2\theta - 1) >$ (θ is the angle between the direction of the bond and the bilayer normal). The values of P_2 represent the lipid bond alignment, where $P_2 = 1.0$ corresponds to perfect alignment with the bilayer normal and $P_2 = 0.0$ corresponds to a random orientation. Since the membrane deformation and pore formation caused by the peptide translocation disrupt membrane order, the higher order of lipid structures in cholesterol systems reduces the sta-

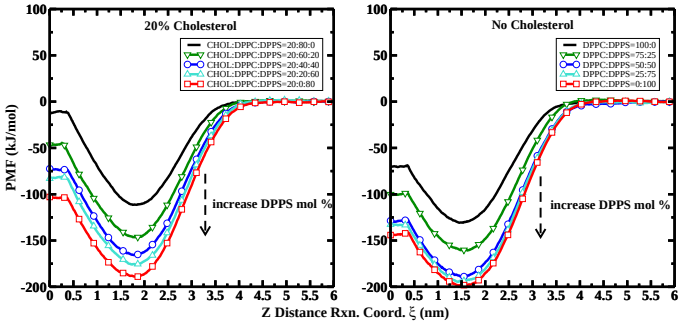

Fig. 14 Total PMF contribution from the system components: DPPS, ions(Na^+ and Cl^-) and DPPC in 20% CHOL and no CHOL mixture systems. (note: water contributions are not included in each curve.)

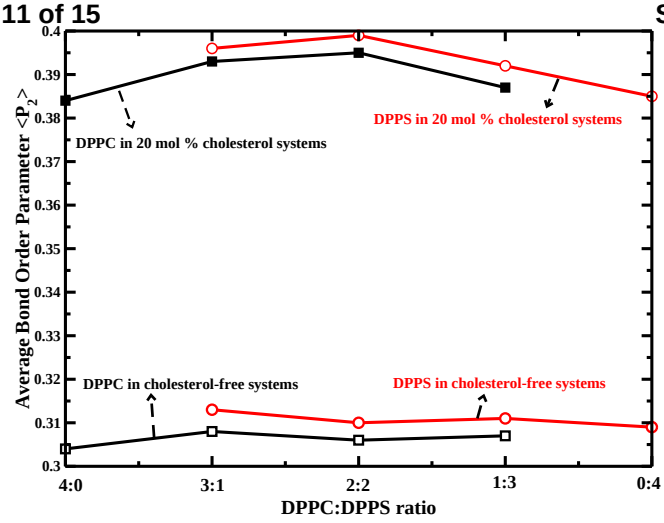

Fig. 15 Average bond order parameter

bilizing contribution from lipids.

Overall, the lipid stabilization effect reduces the translocation barrier of the peptide in the systems, but it is still insufficient to compensate the large free energetic penalty from the combined loss of water, ions and cholesterol interactions.

3.2.3 Peptide Mobility We address peptide permeability in this section. Dynamic permeability, or $log(P_{dynamic})$, which is measured for small molecules, is an often-used experimental observable related to thermodynamic translocation free energy barriers accessible via MD simulations. In practice, procedures such as high-throughput, parallel artificial membrane permeability assays (PAMPA) and cell-based CaCo-2 assays are exploited to measure the dynamic permeability of small molecules. Of course, such methods cannot provide detailed atomistic insights about translocation. Presently, we apply the inhomogeneous solubility-diffusion model[68–70] to estimate TAT dynamic permeabilities using the PMF's and local diffusivity profiles obtained from our MD simulations via the following expression:

$$\frac{1}{P_{dynamic}} = \int_{z_1}^{z_2} \frac{exp[\beta W(z)]}{D(z)}\, dz \qquad (3)$$

where $W(z)$ is the potential of mean force, $D(z)$ is the local diffusivity coefficient, and β is $\frac{1}{k_B T}$.

We used the protocol proposed by Hummer et. al[71,72] to calculate the position-dependent diffusion coefficient D(z) along the membrane normal. Accordingly, the local diffusion coefficient of a single peptide from umbrella sampling MD simulations can be estimated by

$$D = var(z)/\tau \qquad (4)$$

where the relaxation time, τ is obtained by the following equation

$$\tau \approx \left[\frac{nvar(\bar{z})}{var(z)} - 1\right] \Delta t/2 \qquad (5)$$

where, n is the number of data points in each umbrella sampling trajectory, var(z) and var($\bar{z}$) are the variance of z and variance of average z coordinate, respectively, and Δt is time interval between data points.

Unsurprisingly, peptide diffusion is greater in the neutral lipid systems than the anionic mixed systems in the interfacial region (see Fig. 16). This suggests that increasing surface charge in the PS-containing systems weakly changes the mobility of the peptide at the interface. In fact, this is qualitatively consistent with the experimental result. The CLSM images of a single TAT peptide on the GUV surfaces shows that the mobility of TAT on the neutral GUV surfaces is higher than on anionic GUVs; however increasing surface charge has very little impact on TAT mobility on the anionic GUV surface[12]. The rate measured experimentally ($\sim 5 \times 10^{-6} nm^2 \cdot ps^{-1}$) is roughly 10 times slower than the result calculated from our simulations. Since the peptide is bound to a large fluorescence tracer in the experiments, the tracer may slow peptide diffusion on the membrane surface. Furthermore, the experiments were carried out at room temperature, instead of 350 K we used in simulation.

Table 4 and Table 5 show values of computed dynamic permeabilities, $P_{dynamic}$, and $log(P_{dynamic})$ values for zero and twenty percent cholesterol systems with varying PS composition. Consistent with our computed PMF's, the permeabilities are essentially vanishingly small. This is in stark contrast to experimental observations of peptide permeation on the timescales of seconds to minutes[12,73,74]. Though the absolute values of the permeabilities are inaccurate, the general trends follow the PMF profiles. Increasing PS composition of the simulated model membranes decreases barriers and subsequently increases permeabilities; systematically, permeabilities are greater in the cholesterol-free systems relative to the 20 percent cholesterol systems. This is explained through arguments of increased membrane rigidity induced by cholesterol as discussed in earlier sections.

4 Summary

In this work, we have studied the translocation thermodynamics of a cationic TAT peptide across cholesterol-

Table 4 Computed Dynamic Permeabilities from Inhomogeneous Diffusion-Solubility Model. Cholesterol-Free Systems with Varying PS Concentration

Percent PS	$P_{dynamic}$ ($\frac{cm}{sec}$)	$\log(P_{dynamic})$
0.0	7.1 x 10^{-30}	-67.12
25.0	1.4 x 10^{-22}	-50.3
50.0	8.6 x 10^{-20}	-43.9
75.0	4.8 x 10^{-18}	-39.9
100.0	3.8 x 10^{-17}	-37.8

Table 5 Computed Dynamic Permeabilities from Inhomogeneous Diffusion-Solubility Model. 20 Percent Cholesterol Systems with Varying PS Concentration

Percent PS	$P_{dynamic}$ ($\frac{cm}{sec}$)	$\log(P_{dynamic})$
0.0	5.3 x 10^{-35}	-78.9
20.0	3.0 x 10^{-30}	-68.0
40.0	3.3 x 10^{-26}	-58.7
60.0	6.0 x 10^{-24}	-53.5
80.0	4.1 x 10^{-22}	-49.3

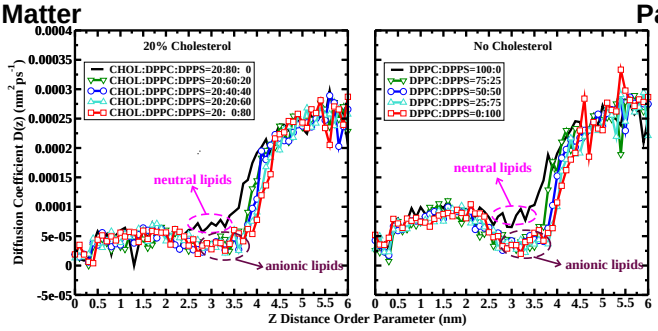

Fig. 16 Local diffusivity profiles for (a) 20% CHOL. in model DPPC/DPPS lipid bilayers with different percentage of DPPS.(b) NO CHOL. in model DPPC/DPPS lipid bilayers with different percentage of DPPS

containing and cholesterol-depleted DPPC/DPPS membrane systems. We estimated the potentials of mean force by using umbrella sampling molecular dynamics simulations coupled to Martini coarse-grained force field. In accordance with experimental observations, we consider the diffusive process of the peptide along a pre-defined Rxn. Coord. ξ describing the z distance between the c.o.m of the peptide and the c.o.m of the membrane. Two major effects, the cholesterol dependence and anionic lipid (or membrane surface charges) dependence, are carefully investigated.

First, by varying the content of cholesterol in DPPC or DPPS lipid bilayers, we observed a systematic change in the translocation PMFs. The addition of cholesterol into membrane increases the barriers of peptide translocation across the membrane. However, the decomposition of the PMFs reveals that cholesterol contributes a weakly destabilizing effect. Further examining the contribution from ions and lipids suggests that the coordination of cholesterol to the peptide replaces some of the lipid binding in the first solvation shell leading to significant decrease of the peptide-lipid interaction. Cholesterol increases the alignment of the lipid bonds to the bilayer normal, which results in a higher order of the lipid molecules.The lipid-ordered phase impedes the reorientation of the lipid molecules. The relatively stiff bonds of the lipid hinders the hydrophilic transmembrane pore formation where lipid reorientation is required. Thus, a large barrier is created in the cholesterol systems. The depletion of cholesterol reduces the translocation cost of the peptide, and favors formation of transmembrane pores. This is in agreement with experimental observations. Comparing the DPPC with DPPS type membrane, our results suggest that the more efficient permeation will occur in the anionic bilayer systems at the same mole percentage of cholesterol or no cholesterol. When there is no cholesterol, the free energy barrier reaches the smallest value in the DPPS-only system. The PMFs also reveal that the change of cholesterol level has a negligible effect on the peptide association to both DPPC and DPPS membranes.

We then systematically changed the mole percentage of anionic lipid DPPS in the presence and absence of cholesterol. The addition of anionic lipids to the neutral bilayer leads to emergence and further enhancement of an interfacially stable state. This is understood by the strong electrostatic interactions between the oppositely charged peptide and lipids. The barrier increases rapidly as peptide moves into the hydrophobic core of the membrane. Decomposition of the PMFs indicates a large penalty from desalting and desolvation of the charged peptide. The reduction of the translocation barrier is directly attributed to the mole percentage increase of DPPS. The preference of the peptide-anionic lipid interaction enhances the stabilization of the whole membrane. As shown in experiments, 40 mol % PS membrane enables rapid internalization of the TAT peptide into GUVs through a transmembrane pore. The PMFs illustrate that once the pore is formed, the peptide translocation proceeds with little free energetic cost. Additionally, we found that the hydrophilic pore size is on the nanometer scale and within the range of experimental estimates. The relative mobility of the peptide on the different membrane surfaces is qualitatively consistent with the CLSM

experiments.

Though we do not claim quantitative agreement with experimental measurements using the coarse-grained force fields described in this study, particularly with regard to permeability values, we emphasize that relative behaviors are captured by the models we use. The coarse-grained (CG) model we use overcomes the time and length scale limitations of all-atom simulations of large biomolecular systems at the cost of reducing the atomic details. More atomic information and accurate energetics may be gained by carrying out expensive full atomistic simulations. We suggest that systematic modifications of the CG force field can lead to further improvements towards more quantitative agreement between the current models and experiments, with the most critical property related to the barriers observed for translocation. Incorporating experimental data on translocation kinetics into the model development is one alternative modification. Furthermore, reevaluation of the degeneracies associated with the types of reaction coordinates used in this study will need to be addressed in the future as well.

In sum, the present results evaluate the cholesterol and anionic lipid effect on peptide translocation, and qualitatively recapitulate the transmembrane pore size and peptide mobility. We emphasize the significant reduction of the barrier heights in the presence of anionic lipid and absence of cholesterol. These findings complement the intricate studies of cell-penetrating peptides permeating through model membrane mixtures and provide complex picture of the interplay of various species. Recently, negatively charged lipids such as PS lipid are found accumulated at the tumor cell membrane surface, due to the overexpression of certain glycosaminoglycans [75–79]. CPPs can be potentially used to selectively target the tumor cells and thus used for cancer diagnosis or delivery of oncologic therapies.

5 Acknowledgment

The authors acknowledge support from the National Science Foundation (CAREER:MCB:1149802). This publication was made possible by computational resources through the Delaware COBRE program, supported by grants from the National Institute of General Medical Sciences - NIGMS (1 P30 GM110758-02) and (5 P30 GM103519-05) in the Departments of Chemistry and Biochemistry and Chemical Engineering at the University of Delaware. S.P. thanks Nikunj Patel for past fruitful discussion and encouragement.

Notes and references

1 A. D. Frankel and C. Pabo, *Cell*, 1988, **55**, 1189–1193.
2 M. Green and P. M. Loewenstein, *Cell*, 1988, **55**, 1179–1188.
3 I. L. Medintz, T. Pons, J. B. Delehanty, K. Susumu, F. M. Brunel, P. E. Dawson and H. Mattoussi, *Bioconjugate chemistry*, 2008, **19**, 1785–1795.
4 B. R. Liu, Y.-w. Huang, J. G. Winiarz, H.-J. Chiang and H.-J. Lee, *Biomaterials*, 2011, **32**, 3520–3537.
5 A. Eguchi, T. Akuta, H. Okuyama, T. Senda, H. Yokoi, H. Inokuchi, S. Fujita, T. Hayakawa, K. Takeda, M. Hasegawa *et al.*, *Journal of Biological Chemistry*, 2001, **276**, 26204–26210.
6 S. Veldhoen, S. D. Laufer, A. Trampe and T. Restle, *Nucleic acids research*, 2006, **34**, 6561–6573.
7 Y. Jiang, M. Li, Z. Zhang, T. Gong and X. Sun, *Current pharmaceutical biotechnology*, 2014, **15**, 256–266.
8 H. M. T. Hitsuda, M. Kitamatsu, A. Fujimura, F. Wang, T. Yamamoto, X. Han, H. Tazawa, A. Uneda, I. Ohmori, T. Nishiki, K. Tomizawa and H. Matsui, *Biomaterials*, 2012, **33**, 4665–4672.
9 R. R. Patlolla, P. R. Desai, K. Belay and M. S. Singh, *Biomaterials*, 2010, **31**, 5598–5607.
10 Y.-L. Tseng, J.-J. Liu and R.-L. Hong, *Molecular pharmacology*, 2002, **62**, 864–872.
11 I. D. Alves, C. Bechara, A. Walrant, Y. Zaltsman, C.-Y. Jiao and S. Sagan, *PLoS One*, 2011, **6**, e24096.
12 C. Ciobanasu, J. P. Siebrasse and U. Kubitscheck, *Biophys. J.*, 2010, **99**, 153–162.
13 Y. Su, A. J. Waring, P. Ruchala and M. Hong, *Biochemistry*, 2010, **49**, 6009–6020.
14 C.-Y. Jiao, D. Delaroche, F. Burlina, I. D. Alves, G. Chassaing and S. Sagan, *J. Biol. Chem.*, 2009, **284**, 33957–33965.
15 A. Walrant, L. Matheron, S. Cribier, S. Chaignepain, M.-L. Jobin, S. Sagan and I. D. Alves, *Anal. Biochem.*, 2013, **438**, 1–10.
16 X. Chen, F. Sa'adedin, B. Deme, P. Rao and J. Bradshaw, *Biochim. Biophys. Acta*, 2013, **1828**, 1982–1988.
17 Y. Rao, S. J. Kwok, J. Lombardi, N. J. Turro and K. B. Eisenthal, *Proc. Nat. Aca. Sci.*, 2014, **111**, 12684–12688.
18 A. Mishra, G. H. Lai, N. W. Schmidt, V. Z. Sun, A. R. Rodriguez, R. Tong, L. Tang, J. Cheng, T. J. Deming, D. T. Kamei *et al.*, *Proc. Nat. Aca. Sci.*, 2011, **108**, 16883–16888.
22 S. J. Marrink and D. P. Tieleman, *Chem. Soc. Rev.*, 2013, **42**, 6801–6822.
19 Y. Hu, X. Liu, S. K. Sinha and S. Patel, *J. Phys. Chem. B*, 2014, **118**, 2670–2682.
20 Y. Hu and S. Patel, *J. Membr. Biol.*, 2014, 1–11.
21 Z. Li, H. Ding and Y. Ma, *Soft Matter*, 2013, **9**, 1281–1286.
23 S. J. Marrink, A. H. D. Vries and A. E. Mark, *J. Phys. Chem. B*, 2004, **108**, 750–760.
24 Y. Hu, S. K. Sinha and S. Patel, *J. Phys. Chem. B*, 2014, **118**, 11973–11992.
25 Y. Hu, S. Ou and S. Patel, *J. Phys. Chem. B*, 2013, **117**, 11641–11653.
26 A. J. Rzepiela, D. Sengupta, N. Goga and S. J. Marrink, *Faraday discussions*, 2010, **144**, 431–443.
27 H. Lee and R. G. Larson, *J. Phys. Chem. B*, 2006, **110**, 18204–18211.
28 S. J. Marrink, H. J. Risselada, S. Yefimov, D. P. Tieleman and A. H. de Vries, *J. Phys. Chem. B*, 2007, **111**, 7812–7824.
29 L. Monticelli, S. K. Kandasamy, X. Periole, R. G. Larson, D. P. Tieleman, and S.-J. Marrink, *J. Chem. Theory Comput.*, 2008,

4, 819–834.
30 M. Seo, S. Rauscher, R. Pomès and D. P. Tieleman, *J. Chem. Theory Comput.*, 2012, **8**, 1774–1785.
31 D. H. de Jong, X. Periole and S. J. Marrink, *J. Chem. Theory Comput.*, 2012, **8**, 1003–1014.
32 G. Singh and D. P. Tieleman, *J. Chem. Theory Comput.*, 2011, **7**, 2316–2324.
33 J. L. Cascales, S. O. Costa, A. Garro and R. Enriz, *RSC Advances*, 2012, **2**, 11743–11750.
34 B. Hess, H. Bekker, H. J.C.Berendsen and J. G.E.M.Fraaije, *J. Comp. Chem.*, 1997, **18**, 1463–1472.
35 S. Kumar, J. M. Rosenberg, D. Bouzida, R. H. Swendsen and P. A. Kollman, *J. Comp. Chem.*, 1992, **13**, 1011–1021.
36 W. Humphrey, A. Dalke and K. Schulten, *Journal of Molecular Graphics*, 1996, **14**, 33–38.
37 K. Huang and A. E. García, *Biophys. J.*, 2013, **104**, 412–420.
38 D. Scherfeld, N. Kahya and P. Schwille, *Biophys. J.*, 2003, **85**, 3758–3768.
39 J. P. Incardona and S. Eaton, *Current opinion in cell biology*, 2000, **12**, 193–203.
40 R. Demel, K. Bruckdorfer and L. Van Deenen, *Biochimica et Biophysica Acta (BBA)-Biomembranes*, 1972, **255**, 321–330.
41 S. Raffy and J. Teissie, *Biophysical journal*, 1999, **76**, 2072–2080.
42 R. A. Demel and B. De Kruyff, *Biochimica et Biophysica Acta (BBA)-Reviews on Biomembranes*, 1976, **457**, 109–132.
43 G. W. Stockton and I. C. Smith, *Chemistry and physics of lipids*, 1976, **17**, 251–263.
44 P. Brûlet and H. M. McConnell, *Proc. Nat. Aca. Sci.*, 1976, **73**, 2977–2981.
45 R. A. Cooper, *Journal of supramolecular structure*, 1978, **8**, 413–430.
46 X. Xu and E. London, *Biochemistry*, 2000, **39**, 843–849.
47 H. Ohvo-Rekilä, B. Ramstedt, P. Leppimäki and J. Peter Slotte, *Progress in lipid research*, 2002, **41**, 66–97.
48 W. D. Bennett, J. L. MacCallum, M. J. Hinner, S. J. Marrink and D. P. Tieleman, *J. Am. Chem. Soc.*, 2009, **131**, 12714–12720.
49 J. A. Hamilton, *Current opinion in lipidology*, 2003, **14**, 263–271.
50 P. Wadhwani, R. Epand, N. Heidenreich, J. Bürck, A. Ulrich and R. Epand, *Biophys. J.*, 2012, **103**, 265–274.
51 M. Di Pisa, G. Chassaing and J.-M. Swiecicki, *Biochemistry*, 2014, ASAP.
52 H. D. Herce and A. E. Garcia, *Proc. Nat. Aca. Sci.*, 2007, **104**, 20805–20810.
53 J. R. Marks, J. Placone, K. Hristova and W. C. Wimley, *J. Am. Chem. Soc.*, 2011, **133**, 8995–9004.
54 Y. Hu, S. K. Sinha and S. Patel, *Langmuir*, 2015, ASAP.
55 P. Saalik, A. Niinep, J. Pae, M. Hansen, D. Lubenets, U. Langel and M. Pooga, *J. Control. Release*, 2011, **153**, 117–125.
56 W. Bennett, N. Sapay and D. P. Tieleman, *Biophys. J.*, 2014, **106**, 210–219.
57 J. Pae, P. Säälik, L. Liivamägi, D. Lubenets, P. Arukuusk, Ü. Langel and M. Pooga, *Journal of Controlled Release*, 2014, **192**, 103–113.
58 W. D. Bennett, J. L. MacCallum and D. P. Tieleman, *J. Am. Chem. Soc.*, 2009, **131**, 1972–1978.
59 T. J. Yacoub, A. S. Reddy and I. Szleifer, *Biophys. J.*, 2011, **101**, 378–385.
60 C. L. Wennberg, D. van der Spoel and J. S. Hub, *J. Am. Chem. Soc.*, 2012, **134**, 5351–5361.
61 K. Simons and W. L. Vaz, *Annu. Rev. Biophys. Biomol. Struct.*, 2004, **33**, 269–295.
62 F. Frézard and A. Garnier-Suillerot, *Biochim. Biophys. Acta*, 1998, **1389**, 13–22.
63 S. Yesylevskyy, S.-J. Marrink and A. E. Mark, *Biophys J.*, 2009, **97**, 40–49.
65 H. Lee and R. G. Larson, *J. Phys. Chem. B*, 2008, **112**, 7778–7784.
66 W. D. Bennett and D. P. Tieleman, *J. Chem. Theory Comput.*, 2011, **7**, 2981–2988.
67 D. Sun, J. Forsman, M. Lund and C. E. Woodward, *Phys. Chem. Chem. Phys.*, 2014, **16**, 20785–20795.
64 W. F. Drew Bennett and D. Peter Tieleman, *Acc. Chem. Res.*, 2014, **47**, 2244–2251.
68 J. M. Diamond and Y. Katz, *J. Membr. Biol.*, 1974, **17**, 121–154.
69 S.-J. Marrink and H. J. C. Berendsen, *J. Phys. Chem.*, 1994, **98**, 4155–4168.
70 C. T. Lee, J. Comer, C. Herndon, N. Leung, A. Pavlova, R. V. Swift, C. Tung, C. N. Rowley, R. E. Amaro, C. Chipot, Y. Wang and J. C. Gumbart, *J. Chem. Inf. Model.*, 2016, **56**, 721–733.
71 G. Hummer, *New J. Phys.*, 2005, **7**, 34.
72 F. Zhu and G. Hummer, *J. Chem. Theory Comput.*, 2012, **8**, 3759–3768.
73 F. Duchardt, M. Fotin-Mleczek, H. Schwarz, R. Fischer and R. Brock, *Traffic*, 2007, **8**, 848–866.
74 G. Tunnemann, G. Ter-Avetisyan, R. M. Martin, M. Stockl, A. Herrmann and M. C. Cardoso, *J. Biol. Chem.*, 2009, **14**, 469–476.
75 M.-L. Jobin and I. D. Alves, *Biochimie*, 2014, **107**, 154–159.
76 K. Matsuda, H. Maruyama, F. Guo, J. Kleeff, J. Itakura, Y. Matsumoto, A. D. Lander and M. Korc, *Cancer research*, 2001, **61**, 5562–5569.
77 J.-h. Lee, H. Park, H. Chung, S. Choi, Y. Kim, H. Yoo, T.-Y. Kim, H.-J. Hann, I. Seong, J. Kim *et al.*, *Journal of Biological Chemistry*, 2009, **284**, 27167–27175.
78 R. D. Sanderson, Seminars in cell & developmental biology, 2001, pp. 89–98.
79 I. Vlodavsky, O. Goldshmidt, E. Zcharia, R. Atzmon, Z. Rangini-Guatta, M. Elkin, T. Peretz and Y. Friedmann, Seminars in cancer biology, 2002, pp. 121–129.

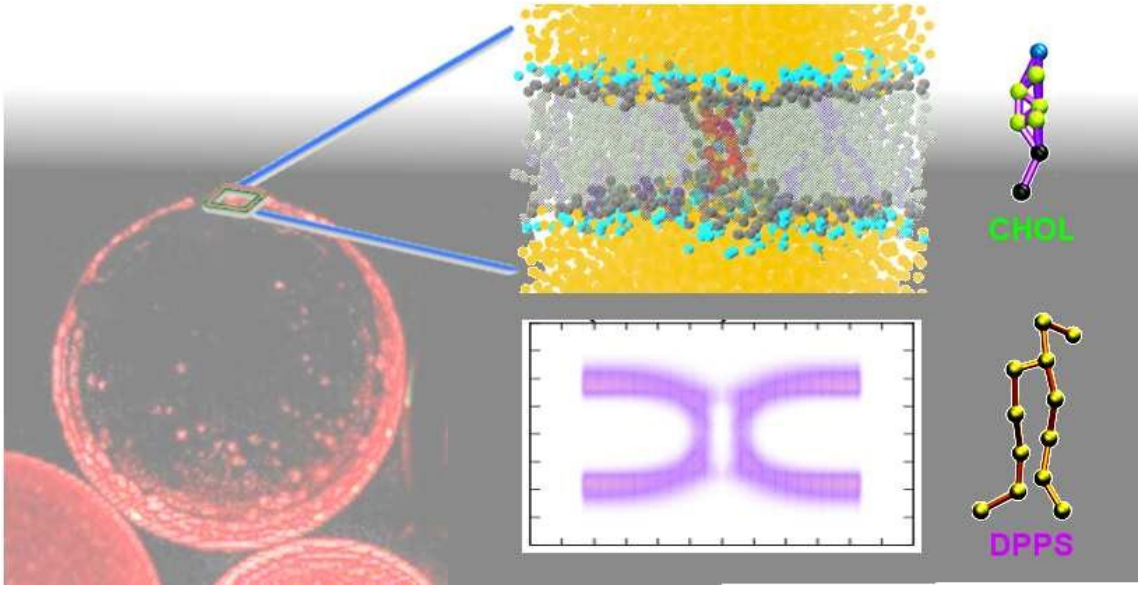

Fig. 17 table of content